

Development of CHF Mapping Method for Fin Structured Surface

Jin Young Choi, Hee Cheon NO*

Department of Nuclear and Quantum Engineering, Korea Advanced Institute of Science and Technology, 291 Daehak-no, Yuseong-gu, Daejeon, Republic of Korea
cjy0215@kaist.ac.kr; hcno@kaist.ac.kr

ABSTRACT

Several factors have been identified to affect CHF enhancement: wettability, surface roughness, porosity, surface structure and so on. In this study, we performed CHF experiments using structured surfaces to validate the parameter effects and to understand their physical meanings. Experimental results show that the CHF has a peak value as fin geometry change. A fin with 0.5mm height produces a largest CHF around 1.9MW/m^2 , and fins longer than 2mm reduced CHF values. To explain the results, we developed a CHF mapping method describing liquid supply-side and demand-side limits. The liquid demand-side limit is governed by heat removal capability, mainly nucleates boiling at the heating surface and calculated using the hot spot model. We consider 3 liquid supply-side limiting mechanisms limiting liquid supply to the heating surface: capillary limit in the fin structure and CCFLs in the fin structure and free volume. The capillary limit is determined by balancing capillary pressure and viscous dissipation in liquid film on the fin side. The CCFL in the structure is calculated using a Wallis-type correlation. The CCFL in the free volume limits liquid downward flow by the vapor jetting from the heating surface. The CHF map drawn for our experimental results describes the CHF trend in the water pool successfully. Also, we show that the CHF mapping method well explain the experimental trend in terms of fin length using FC-72 as a bulk liquid. As a result, it is proven that the CHF mapping is an effective way of explaining the CHF in a pool boiling.

KEYWORDS

Critical Heat Flux, fin structure, Liquid demand-side limit, Liquid supply-side limit, CHF map

1. INTRODUCTION

Nuclear safety issues related to the severe accident are arisen recent years due to the Fukushima accident, especially on the passive heat removal system for the large fuel failure. Since present nuclear power plant safety system generally removes the decay heat by auxiliary feed water system with active pump, there should be electricity after the accident occurs. However, from the Fukushima accident, it is shown that when the station blackout occurs, it is not able to maintain the electricity by failure of a power transmission structures. To secure the safety at beyond design basis accidents, ex-vessel cooling is suggested to remove the decay heat by passive injection system and boiling heat transfer. The system is effective and independent of the electricity and the reliability is high at the severe accident. But, large light water reactors require heat removal capability that the required heat flux can be higher than conventional CHF. Therefore, we need to enhance the CHF to increase their heat removal capacity. There exist various CHF enhancement methods such as surface treatment, fluid property or flow rate control and so on. Among them, we focus on the controlled surface treatment for CHF enhancement due to its degree of enhancement, robustness, and predictability.

In this study, we develop a CHF mapping method to understand the CHF mechanism and find an optimal surface design for finned structure. The map is drawn with liquid supply-side and demand-side limits: the capillary force, countercurrent flow limit, and hot spot model are considered and quantified with the validation of CHF experiments.

2. CHF EXPERIMENT

Pool boiling experimental tests are conducted to observe the CHF trends for various fin structures. We expect that they will show the individual parametric effects by controlling geometric variables.

2.1. Experimental Apparatus and Procedure

A boiling tank (320x400x400mm) of 40L water capacity is made by a polycarbonate. Two copper columns are attached to the lid of water tank for connection of a test section and a rectifier. There is a small hole at the lid to put a rubber tube led to the empty bucket for maintaining an atmospheric pressure inside the tank. Fig. 1 shows the simple schematic drawing of a boiling tank.

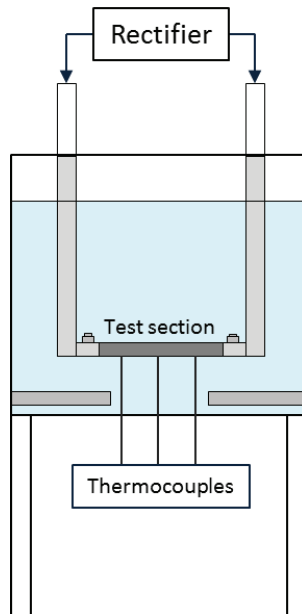


Figure 1. Schematic of boiling pool and measurement apparatus

A rectifier (3000A, 10V / 1700A, 36V) is connected to the test section through electric wires and copper column. We performed tests using two different rectifiers due to some problems in the laboratory condition. A test section consists of specimen, supporting Bakelite and copper board as a connecting part to the copper column fixed by bolts. At a lower surface of the specimen, three K-type thermocouples are installed at center, right side and left side covered with a high-temperature silicon to remove a heat generated only through an upper surface. A gap between supporting Bakelite and specimen is also filled with a high-temperature silicon to avoid water trespassing into the lower surface. Specimens of 15x50mm size with 2mm-base thickness are made by Stainless Steel 304 with various fin structures on surface fabricated by EDM (Electro Discharge Machining) process. Table I shows the fin geometry data of various specimens.

Table I. Test matrix for experiment

Fin size	1mm x 1mm							
Gap distance(mm)	1	0.7	1	2	1			
Fin length(mm)	0.2		0.5		0.7	1	2	3

Bulk temperature is set to the saturation temperature during a whole test time using two cartridge heaters (0.5kW each) under the test section. Specimen temperature is measured through the thermocouples installed under the specimen and a voltage is checked at the top of the copper column to reflect a voltage drop through the electrical wires. The current value is provided from the rectifier. The measured values are recorded on the computer by data acquisition systems. We set the program for controlling the current to raise the power regularly and identically for all of the specimens. Current is raised by 10A for every minute up to the first 30 minutes and 5A for every minute after then. The CHF point is determined when the temperature sharply rises for few seconds. We calculated heat flux by multiplying a current and a voltage and dividing it by the specimen base area (15x50mm) considering it as surface area. An upper surface of specimen temperature is necessary for heat transfer coefficient calculation. As we have a lower surface temperature through three thermocouples, we calculated the upper surface temperature at CHF by considering the thermal conductivity of Stainless Steel 304 and Joule heating capacity. The calculated upper surface temperature is an average value of the bottom temperature since we suppose that CHF initiates at the bottom surface, not at the fin structure.

2.2. Experimental Results

The experimental results include the CHF values and the surface temperatures at CHF. Fig. 2 shows the averaged CHF values from rectifier 1 and 2 versus the fin length with the 1mm-gap distance.

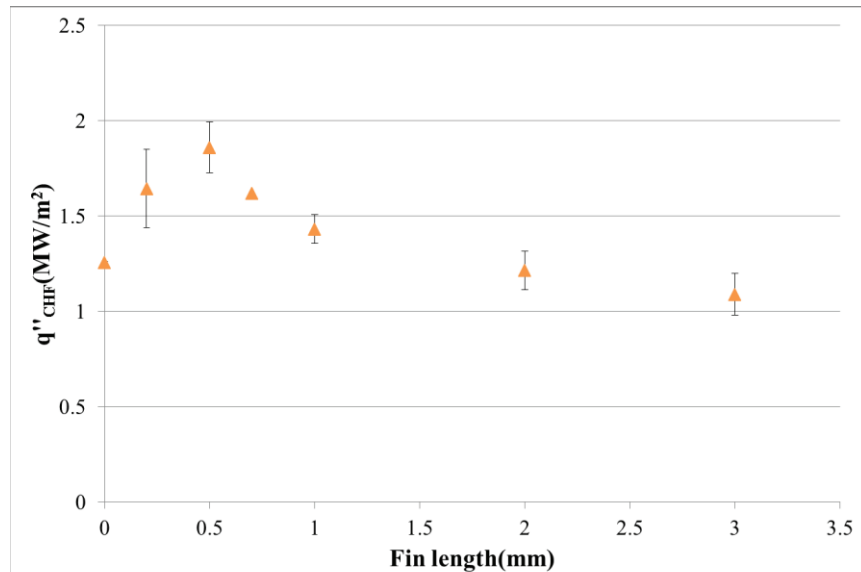


Figure 2. Experimental CHF values versus fin length for 1mm-gap distance

As shown in the graph, the change of fin length has a strong influence on the CHF with a specific trend. When the fin length is shorter than 0.5mm, CHF increases as the fin length increases. If the fin length is

higher than 0.5mm, CHF decreases. When a fin is longer than 2mm, CHF drops even to the smaller values than that of the surface without fin structures. The results do not show the expectation that CHF would increase due to its extended surface area as the fin length increases. Fig. 3 shows the CHF values upon the apparent surface area ratio.

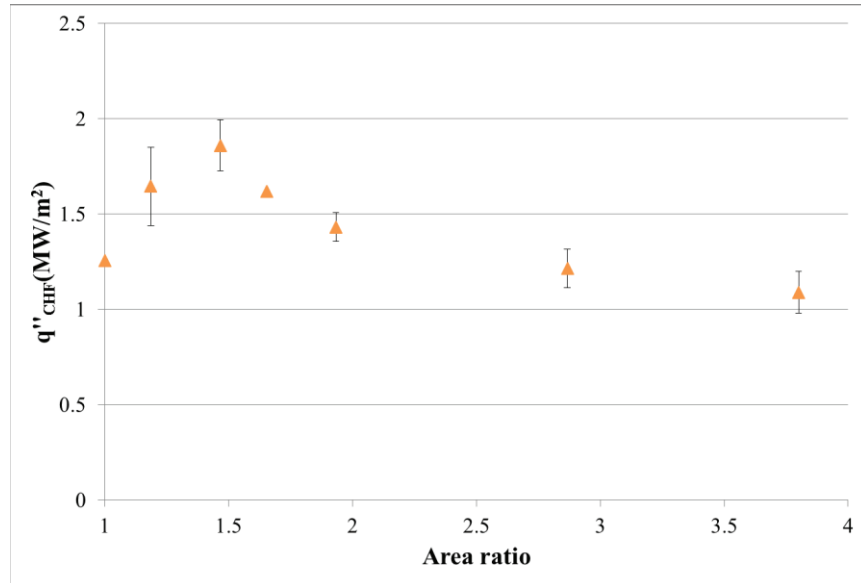


Figure 3. Experimental CHF values versus surface area ratio for 1mm-gap distance

The graph represents that the area ratio is affecting CHF giving a peak value around the area ratio of 1.5. In section 3, we will propose the CHF map method applicable to CHF in the fin structures.

3. CHF MECHANISM ANALYSIS

3.1. CHF map development

In order to explain our experimental results, we propose a CHF mapping method for limiting mechanisms like a heat pipe performance map. A heat pipe is another heat exchanging system operated by a balance of a liquid supply and a vapor formation rate for the surface heat removal. The system is led to failure by limiting mechanisms such as capillary, boiling and entrainment limit when its power exceeds the allowed range. We referred to the concept of limitation map and mechanisms of the limitations from the heat pipe system. Since the capillary limit and entrainment limit well describe the liquid-vapor countercurrent phenomenon in the fin structure, we included those factors in consideration.

A fundamental idea of our study is that the CHF is determined by various mechanisms which limit the heat removal capability, mainly by continuous nucleate boiling. We draw the map showing limiting lines limited by liquid demand-related mechanisms and by liquid supply-related ones. The shape of each line can be changed since various parameters affect each limit in different ways. There can be a certain parameter which increases a liquid demand-side limit as it is getting bigger. Another parameter decreases liquid demand-side limit as it is getting larger. Figure 4 shows the simple example of a CHF map.

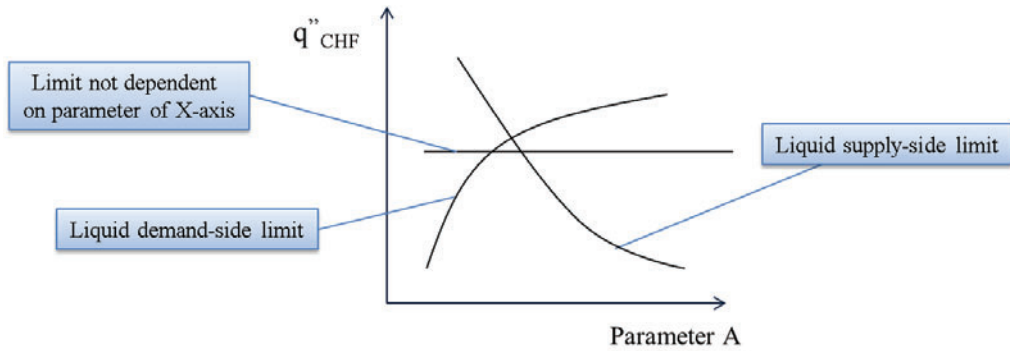


Figure 4. Simple example of CHF map

The detailed explanations of the limits will be followed.

3.1.1. Liquid demand-side limit

In the current model the liquid demand-side limit means that the superheat of the surface generates irreversible hot spots and initiates CHF, even though there exists enough liquid supply to the surface. From our previous research, Choi and NO [1], it is shown that the effective surface area well represents the CHF by nucleate boiling limitation. The effective surface area model is a method to convert fin structures into the effective heat removal area by using thermal conduction and heat transfer coefficient calculating fin efficiency. The model can be applied to the hot spot model by extending base surface area since the hot spot model does not consider the structured surface. Additionally, we should consider the contact angle representing the wettability. The limit is applied only when there exists sufficient liquid supply to the boiling region. In section 3.2.1, detailed calculation method of the model will be shown.

3.1.2. Liquid supply-side limits

On the other hand, liquid supply-side limits mean the lack of the liquid supply compared to the liquid demand. If the liquid supply is not enough to rewet the dry spots after the bubble departure, regular dry spots can be irreversible ones limiting the heat removal capability. The liquid supply-side limits are related to hydraulic phenomena such as a countercurrent flow limit (CCFL) and a capillary limit. Also, the countercurrent flow limit is categorized into two parts: CCFL in the free volume and in the structure.

The CCFL in the free volume limits the liquid supply reaching the top of the structure. From the phenomenon, the liquid flow falling down from the pool is limited by the jetting vapor flow generated from the heating surface through wave instability such as Kelvin-Helmholtz instability. If it happens, the limited amount of liquid reaches the top of the structure.

The CCFL in the fin structure limits the liquid supply reaching the bottom of the heating surface. By the CCFL, the bubble departing from the bottom surface blocks liquid inlet to the bottom surface if the bubble velocity is high enough. In order to evaluate the liquid flow reaching the bottom of the heating surface, we can use a Wallis-type CCFL correlation [2] expressed in terms of each fluid velocity, density, gravity and width of liquid path.

The capillary limit is governed by the balance between the capillary force and the viscous dissipation force. When liquid flows into the bottom surface, it forms liquid film on the fin side due to steam flow. In that case, capillary pressure drives the liquid flow, while the viscous dissipation inhibits the liquid flow.

The capillary pressure and dissipation forces are expressed in terms of effective radius, latent heat, liquid path length, and so on.

Both of the CCFL in the structure limit and the capillary limit are related to limiting the liquid supply rate into the fin structure. If the CCFL in the structure limit is lower than the capillary limit, the liquid supply rate into the fin structure is limited by the CCFL in the structure limit. On the other hand, if the capillary resistance is high enough, the liquid supply rate into the fin structure is restricted by the capillary limit.

3.2. CHF Mapping on CHF Experiments in the Water Pool

A sketch of a CHF map is shown in section 3.2. We applied our experimental results to our CHF map in terms of the fin length to obtain the optimal fin length. In case of the lengthened fin, the liquid supply by capillary pressure is lowered and the area for nucleate boiling is extended. Accordingly, the liquid demand-side limit increases and the liquid supply-side limit decreases as a fin length becomes longer. As a result, a shape of the CHF map will be similar to Fig. 4. As shown in Fig. 4, for short fins, the liquid demand-side limit, a surface area extension or surface wettability, becomes a main factor of CHF determination. On the other hand, for long fins, the liquid supply-side limit, capillary flow dissipation, acts as a main determination factor of the CHF. In the following subsections, the limits stated above will be developed upon the fin length change.

3.2.1. Liquid demand-side limit – Hot spot/Effective Extension Area Model

According to the Ha and No hot spot model [3-5], CHF can be described as an extension of nucleate boiling with an increase in the dried area leading to a peak of the wall heat removal capacity as the wall temperature increases. The model describes nucleation sites which are distributed by Poisson distribution. Also, in the model, irreversible dry spot is formed when the spot is surrounded by certain number of nucleation site due to liquid transfer is blocked. As a result, as CHF is governed by the maximum heat removal capability, we can say that the Ha and No model represents the limit of the liquid demand side, rather than the liquid supply side. In order to develop the liquid demand-side CHF model in the fin structure, the Ha and No's hot spot model developed for CHF on the bare heating surface is extended to introduce the effective extension area concept as described in our previous study [1]. The method adopted fin effectiveness considering temperature gradient through the fin and calculated a net amount of heat removal from the fin and surface. By the method, it is possible to expect the practical effect of structures for heat removal. In this extended hot spot model, the heating area of the bare surface is extended into the effective extension area. CHF in the fin structure is obtained by CHF estimated by the hot spot model without the fin structure multiplied by the effective extension area ratio.

A distinguishing aspect of our experimental results is the existence of a peak CHF value as the fin length increases. To explain the phenomenon, we firstly analyzed the results using the effective extended surface area model. The study suggested the effective surface area calculation method adopting a fin efficiency,

η_0 and axial fin temperature gradient. The method uses apparent surface area and base temperature for prediction of the CHF. The following equations represent the calculation method of the extended hot-spot model:

$$\frac{\theta_x}{\theta_b} = \frac{\cosh m(L-x) + (h/mk) \sinh m(L-x)}{\cosh mL + (h/mk) \sinh mL} \quad (1)$$

$$\eta_f = \frac{q_f}{q_{\max}} = \frac{q_f}{hA_f\theta_b} \quad (2)$$

$$q_f = hA_f\theta_x \quad (3)$$

$$\eta_0 = 1 - \frac{A_f}{A_t}(1 - \eta_f) \quad (4)$$

where $m^2 = hp/kA_c$, $\theta_x = T(x) - T_\infty$ and $\theta_b = T_b - T_\infty$, and x is an axial distance from bottom surface along the fin.

To calculate the CHF ratio, η_0 is multiplied by the actual extended surface area ratio of the fin. We demonstrated that the proposed method well predicted the experimental results performed by Chih Kuan Yu and Ding Chong Lu [6]: an increase in an extended surface area ratio is quantitatively well matched with a CHF enhancement ratio. Their experiment used FC-72 as bulk fluid and a copper heater with millimeter-scale fin structures. However, when the extended surface area model is applied to our experimental results, the predicted CHF values are not in good agreement with our experimental ones as shown in Fig. 5. The CHF ratio is a relative CHF value of the structured surface to the CHF of the bare surface.

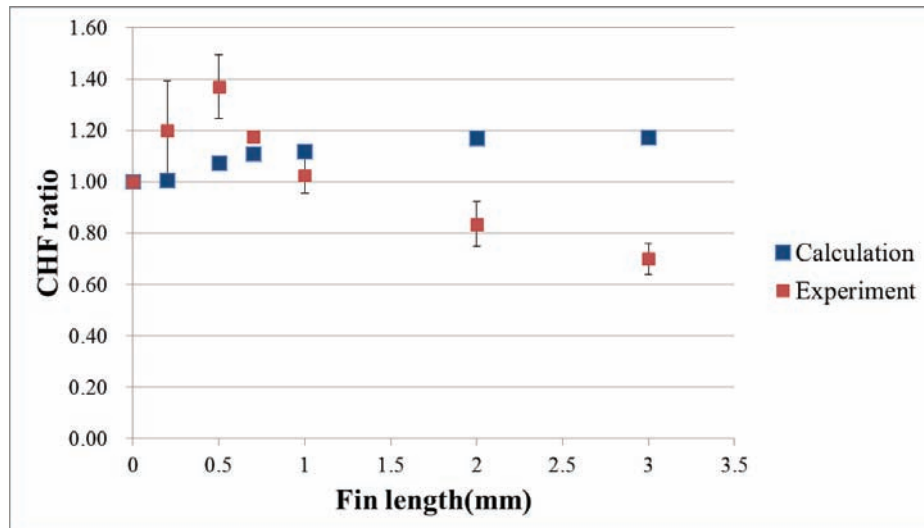


Figure 5. Comparison of predicted CHF ratio by effective surface area method with experimental one versus fin length

As shown in the graph, the effective surface area model does not follow our experimental results well. The predicted values continuously increase as fin length increases while the experimental results show a peak value. For the fins shorter than 1mm, the experimental CHF values are much higher than the predicted ones. For the fins with the fin length longer than 2mm, the trend becomes reversed. The main roles of the fin structure for heat removal system are to extend the surface area for nucleate boiling and to distribute base superheat to the fin structures to reduce the bottom surface temperature for the same heat flux.

As shown in Fig. 5, the effective surface area model without considering the contact angle of the finned surface predicted lower CHF than the experimental results for the short fins. Therefore, we measured contact angles for various fin lengths and calculated contact angle effect.

The contact angles of the finned structures are measured with Pheonix 300+/ LCA10 for specimens with various fin lengths using water. We measured the contact angles repetitively for each sample to secure the accuracy of the measured values. Table II shows the measured contact angles for various fin lengths. The amount of water droplet is varied from 3um to 20um which is dropped on the center of the space among four fins. The droplet is shown to be contacting with the side surfaces of the fins.

Table II. Measured contact angles

Fin length	Contact angle(°)
0	90.6
0.2	75
0.5	67
1	81.4

The measured contact angle increases as the fin length increases when the fin length is smaller than 0.5mm while it increases again with around 1mm. The trend is similar to the experimental results, which have a peak value. This is thought to be related to the fin structure and liquid film contact to the fin surface. Based on the measured data, the fin structure with 0.5mm-length is an optimal geometry to spread the water film. For specimens with fins longer than 1mm, contact angles are not measurable due to the liquid absorption among the fins.

In order to implement the effect of the contact angle on CHF quantitatively, we put the measured contact angles into the hot spot model calculating CHF. In the hot spot model, contact angles is taken into account to calculate the nucleate site density as shown in Eq. 5:

$$\bar{N}_0 = 5 \times 10^{-27} (1 - \cos \theta) / d_c^6 \quad (5)$$

where the cavity diameter, d_c , is related to the surface superheat. Fig. 6 shows the calculation results compared to the experimental results.

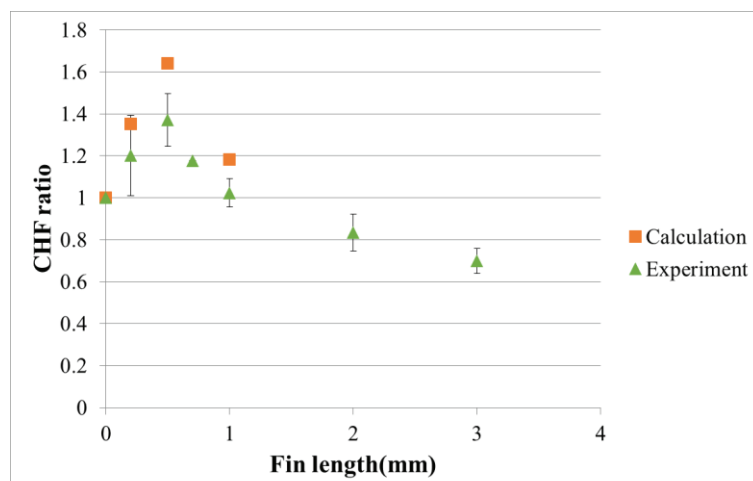


Figure 6. CHF ratios calculated by hot spot model using measured contact angles and experimental data versus fin length

As shown in the graph, the contact angles can reflect the experimental results well. The current model shows a peak value at 0.5mm of the fin length which is similar to the experimental CHF trend.

The nucleate site density value is used to calculate a boiling heat flux and dry area fraction. When the nucleate site density is higher than certain number, there forms irreversible dry spots surrounded by neighbor bubbles and CHF occurs. Therefore, the nucleate site density is important for deciding CHF point.

Finally, by comparing the results of extended surface area method and contact angle calculation, it is shown that the wettability effect is more important for liquid demand-side limit in this test condition.

3.2.2. Liquid supply-side limit - Capillary limit

In our research, the capillary limit appears as a key mechanism of the CHF. The capillarity of our experiment is described as the liquid film flowing to the bottom of the surface through the gap between bubble and the fin side as shown in Fig. 7. A liquid film thickness is obtained using the Eq. 6 [7]:

$$\delta_i / D = 0.67 Ca^{2/3} / (1 + 3.13 Ca^{2/3} + 0.504 Ca^{0.672} Re^{0.589} - 0.352 We^{0.629}) \quad (6)$$

where $Ca = \mu U / \sigma$, $Re = \rho U D / \mu$ and $We = \rho U^2 D / \sigma$.

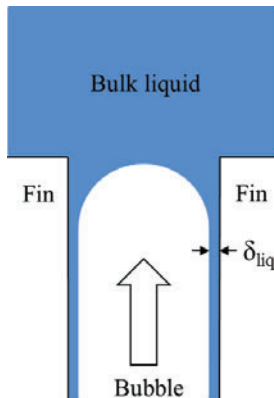


Figure 7. Schematic diagram of the bubble and liquid film

The vapor velocity is calculated regarding that all amount of heat from the bottom surface is transferred to the liquid-vapor phase transition in saturation condition. Calculated liquid film thickness is used as an effective capillary radius. The capillary limit occurs when the amount of liquid supply to the bottom is not enough, particularly for the longer fins. For the longer fins, the capillary frictional pressure of the liquid increases as the path length increases. We calculated the capillary liquid supply-side limit by balancing the frictional or gravitational pressure drop and capillary pressure. Eq. 7 shows the capillary force balance equation and Eq. 8 is a simply rearranged form for the CHF estimation by the capillary limit.

$$\Delta p_c = \frac{2\sigma \cos \theta}{r_{eff}} = \rho_f g H + H \left(\frac{\mu_l \dot{m}}{KA_w \rho_l} \right) + H(f \cdot Re)_v \left(\frac{\mu_v \dot{m}}{2r_{hv}^2 A_v \rho_v} \right) \quad (7)$$

$$q'' = \frac{(\frac{\sigma \rho_v h_{fg}}{\mu_v}) \cos \theta}{4} \cdot \left(\frac{r^2}{r_{eff} H} \right) \varepsilon \quad (8)$$

where $K = 2\varepsilon(r_h)^2 / f_l \cdot \text{Re}_l$, $(f \cdot \text{Re})_v = 16$, $(f \cdot \text{Re})_l = 15$ and $r_{hv} = 2\varepsilon\delta / (\omega + 2\delta)$, and porosity ε is set as 0.5 since both of fin width and gap distance are 1mm.

We calculated the capillary force-limited CHF values. The calculated and experimental results are shown in Fig. 8.

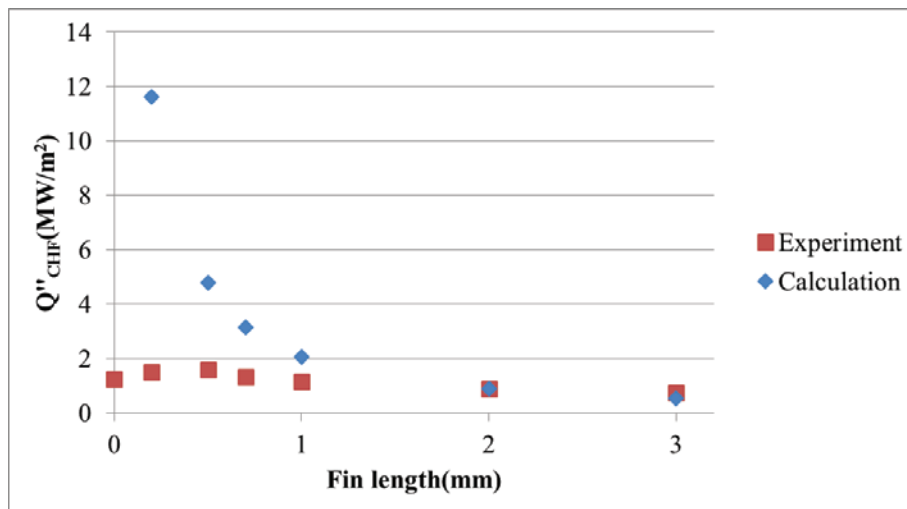


Figure 8. Calculated CHF values for capillary limit and experimental data versus fin length

Since a frictional pressure drop increases as a liquid flow path length becomes longer, the capillary limit exponentially falls down as fin length increases. Therefore, a capillary limit mechanism can explain the low CHF values for long fins in spite of large extended surface area. This means that an increased amount of heat by the surface area extension cannot be fully removed due to limited liquid supply. Even if the finned surface with longer fin length has the larger extended area, CHF can be lower than that of the plane surface: the finned surface with longer fin length can produce negative impact on CHF.

3.2.3. Liquid supply-side limit - CCFL in the free volume

Kutateladze [8] developed a stable film boiling condition by studying the case of pure hydrodynamic detachment of liquid by gas jetting through the microporous plate. The liquid detachment was confirmed by disappearance of the electricity conduction between a metallic microporous plate and a thin wire located parallel to the plate at 0.1 mm above it. He proposed a film collapse model describing the stable gas film collapse criteria:

$$K_s = 30M^{2/3} \quad (9)$$

$$M^2 = \rho_g g A / P \quad (10)$$

$$Ar = g A^3 / \nu^2 \quad (11)$$

$$A = \left[\sigma / g(\rho_l - \rho_g) \right]^{0.5} \quad (12)$$

$$(j_g)_{film} = K_s \sqrt{\sigma / \rho_g A} \quad (13)$$

From the correlations, we obtained 1.33MW/m^2 of CHF by converting the vapor flow rate into the heat flux. Kutateladze obtained the limiting superficial gas velocity by an experiment with a perforation ratio of 0.125. In order to obtain the actual value for our experiment, we should know the void fraction of the pool boiling free volume and calculate the value for that void fraction. An experiment of Andrew Lerch [9] found that the void fraction for the water pool boiling is over 0.5 near the CHF. Based on the void fraction, the free volume liquid supply-side limit reaches about 5.3MW/m^2 .

3.2.4. Liquid supply-side limit - CCFL in the structure

In order to estimate CCFL in the fin structure, we use the Wallis-type correlation [2] in which it is not dependent on the pipe length but to the path diameter:

$$(j_g^*)^{1/2} + M(j_l^*)^{1/2} = C \quad (14)$$

where M and C are constants and $j_k^* = \frac{\rho_k^{1/2} j_k}{[gL(\rho_l - \rho_g)]^{1/2}}$.

The CCFL limit is calculated by equalizing the liquid mass flow rate determined by the amount of vapor and CCFL by the Wallis correlation, Eq. 14. For the experimental results, we need to know the CCFL constants for the 1mm-gap distance. However, since the exact constants M and C for CCFL calculation is not clear in millimeter-scale fluid length, we only estimate the possible range of the CCFL limit. The researches we referred are done by Ghiassian et al. [10] and JH Jung et al. [11]. Ghiassian et al. [10] obtained the constants of $M=0.66$ and $C=0.6$ for the path diameter of 12.7mm. JH Jung et al. [11] obtained the constants of $M=1.22$ and $C=1.7$ for the 2.5mm gap size. The hydraulic diameter is 0.0025m^2 which is calculated by setting the flow path among the four fins as a unit area.

Table III. CCFL limit

Gap size	0.0025 (Hydraulic diameter)	
	$M=1.22, C=2.7$	$M=0.66, C=0.6$
$Q''_{CHF}(\text{W/m}^2)$	43,379,975	2,499,649

Both of the CHF values calculated by CCFL limits are well above the liquid demand-side limit. We safely say that the CCFL limit in the fin structure is not a limiting mechanism of CHF.

3.2.5 CHF mapping results

In the above sections, we developed a CHF map in terms of fin length. The CHF values were calculated considering surface structure geometry and fluid properties to show the liquid demand-side and supply-side limits. Now, we draw a CHF map for our experimental results following the CHF mapping method described in the previous section as shown in Figure 9. The limit based on the hot spot model with an

effective extension area method is a liquid demand-side limit taking account contact angle into calculation representing the experimental results of short fins. The results of the capillary limit shows that the CHF ratio rapidly decreases as the fin length increases. They become comparable with experimental ones when the fin length is larger than 2mm. The line for the CCFL in the structure limit represents a calculation result by putting $M=0.66$ and $C=0.6$. Since the constants are not accurately known, we draw a most conservative CCFL value. We expect that the actual one can be higher than the drawn line. Also, CCFL limit in the free volume is a conservative limit since the void fraction range near the surface would be higher than 0.5.

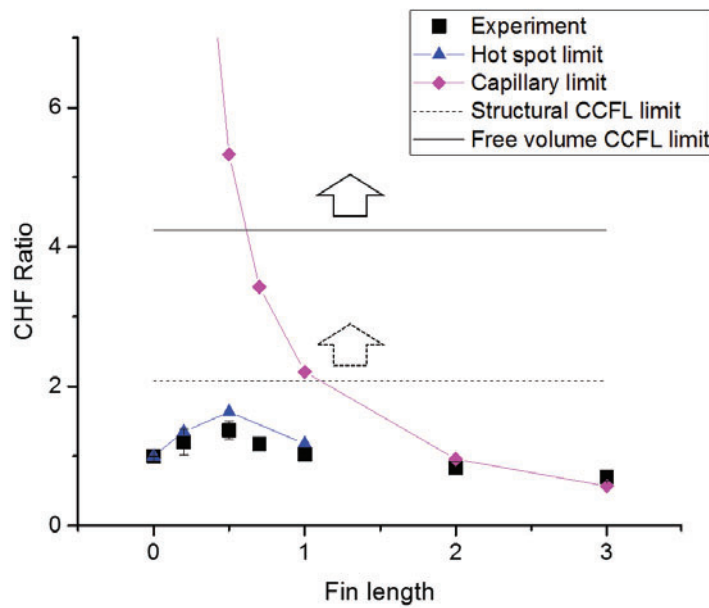


Figure 9. CHF map for experiment of structured surface (SS304) using water

3.3. CHF Mapping on CHF Experiments in the FC-72 Pool

In order to validate the current CHF mapping method further, we draw a CHF map for the experiment of Chih Kuan Yu and Ding Chong Lu [2] as shown in Figure 10. Since the contact angle of FC-72 is generally very small for most materials, almost less than one degree, we excluded the effect of contact angle upon the calculation. Therefore, the CHF values are calculated by an effective extended area method without considering the variation of the contact angle. And we chose lower bounded CHF values for the CCFL limits in the structure and the free volume in the same way as the water CHF mapping described in the previous section. The calculation results show that the FC-72 CHF for the structured surface made by copper is mainly determined by the liquid demand-side limit up to the fin length of 4mm. Since the liquid supply-side limits are much larger than the liquid demand-side limit, we can say that CHF is limited by the heat removal capability by nucleate boiling.

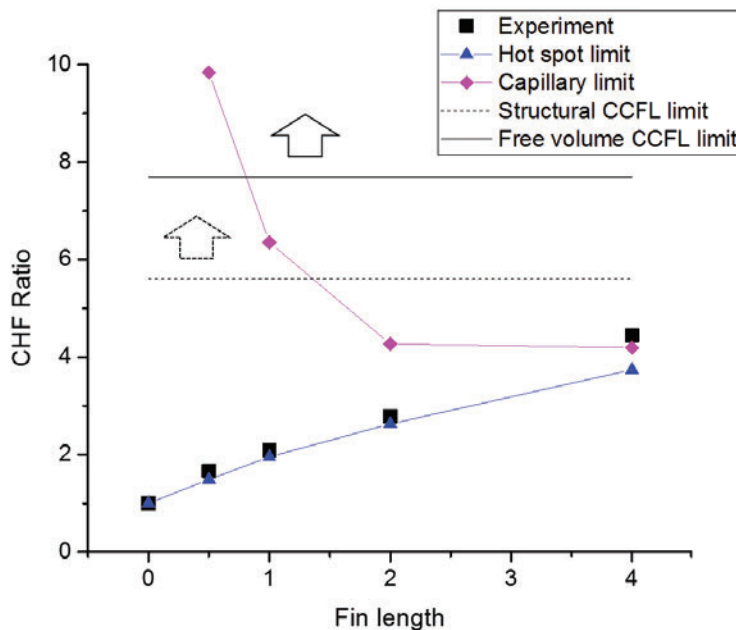


Figure 10. CHF map and experimental CHF with fin structured surface (Cu) using FC-72

4. CONCLUSIONS

In order to find the parametric effect of the fin structure on CHF enhancement, we conducted experiments with finned surfaces. The experimental results show that there exists a peak value of CHF as the fin length increases. The CHF mapping method is proposed to analyze the experimental results. The method describes the CHF by heat removal capability limitation through various limiting mechanisms.

In the CHF map the liquid demand-side limit can be calculated using the extended hot spot model considering the contact angle and the effective extended surface area. The model predicted the experimental results closely. The capillary limit follows the experimental CHF trend for the longer fins. Since the Wallis-type CCFL model in the fin structure does not depend on the flow path length, the constant line for it is drawn in the map. The liquid supply-side limit in the free volume is calculated to be 5.2 MW/m^2 by the Kutateladze model. Also, we drew a CHF map for another experiment using FC-72 as bulk liquid and copper as heating surface. The map describes the results successfully. In conclusion, the CHF mapping method can be utilized to predict CHF and to perform the optimal design of fin structure for the pool design with various fluid materials and fin structure heaters.

NOMENCLATURE

h	Convective heat transfer coefficient($\text{W/m}^2 \cdot \text{K}$)	ρ	Density(kg/m^3)
k	Thermal conductivity($\text{W/m} \cdot \text{K}$)	h	Heat transfer coefficient($\text{W/m}^2 \cdot \text{K}$)
A_f	Fin surface area(m^2)	θ	Contact angle($^\circ$)
A_t	Total surface area(m^2)	d_c	Cavity diameter(m)
A_c	Fin cross-sectional area(m^2)	σ	Surface tension(N/m)

η_f	Fin efficiency	U	Velocity(m/s)
η_o	Overall efficiency	r_{eff}	Effective capillary radius(m)
L	Fin length (m)	h_{fg}	Latent heat(kJ/kg)
D	Diameter (m)	f	Friction factor
δ	Liquid film thickness(m)	j_k	Superficial velocity(m/s)
μ	Dynamic viscosity(Pa·s)	A_v	Vapor flow surface area(m ²)
\dot{m}	Mass flow rate(kg/s)		

ACKNOWLEDGMENTS

This work was supported by the National Research Foundation of Korea (NRF) grant funded by the Korea government (MSIP) (No.2013M2A8A1038479).

REFERENCES

1. Jin Young Choi, Hee Cheon NO, "Analysis of CHF enhancement by heater surface fin structure ranging from micrometer-fin scale to centimeter-fin scale", *Proceedings of ICAPP*, Nice(2013).
2. G.B. Wallis, "One-Dimensional Two-Phase Flow", McGraw-Hill(1969).
3. Ha Sang Jun, Hee Cheon NO, "A dry spot model of critical heat flux in pool and forced convection boiling", *International Journal of Heat and Mass Transfer*, **41**, 2, pp. 303-311(1998).
4. Ha Sang Jun, Hee Cheon NO, " A dry spot model for transition boiling heat transfer in pool boiling", *International Journal of Heat and Mass Transfer*, **41**, pp. 3771-3779(1998).
5. Ha Sang Jun, Hee Cheon NO, " A dry spot model of critical heat flux applicable to both pool boiling and subcooled forced convection boiling", *International Journal of Heat and Mass Transfer*, **43**, pp. 241-250(2000)
6. Chih Kuang Yu, Ding Chong Lu, "Pool boiling heat transfer on horizontal rectangular fin array in saturated FC-72", *International Journal of Heat and Mass Transfer*, **50**, pp. 3624-3637(2007).
7. Younghae Han, "Measurement of the liquid film thickness in micro tube slug flow", *International Journal of Heat and Fluid Flow*, **30**, pp. 842-853(2009).
8. S.S. Kutateladze, "Boiling and bubbling heat transfer under free convection of liquid", *International Journal of Heat and Mass Transfer*, **22**, pp. 281-299(1979).
9. Andrew Lerch, "Measurement of near-surface void fraction and macrolayer thickness in boiling water and silica-based nanofluid", MIT(2008).
10. S.M. Ghiassian, "Countercurrent flow limitation in inclined channels with bends", *Nuclear Engineering and Design*, **152**, pp. 379-388(1994).
11. Ji Hwan Jung, Seung Jin Lee, Rae Joon Park, Sang Baek Kim, "The effect of gap size on counter current flow limitation phenomena in narrow annular gaps with large diameter", *Journal of the Korean Nuclear Society*, **34**, pp. 396-405(2002).